## ORIGINAL ARTICLE

# Adsorption behavior of 8,9-bis(4 (dimethyl amino) phenyl)benzo[4,5]imidazo[1,2-a]pyridine-6,7-dicarbonitrile on mild steel surface in 1 M HCl

## Chandrabhan Verma, M.A. Quraishi *

*Department of Chemistry, Indian Institute of Technology, Banaras Hindu University, Varanasi 221005, India*

**Abstract**  The effect of 8,9-bis(4 (dimethylamino)phenyl)benzo[4,5]imidazo[1,2-a]pyridine-6,7-dicarbonitrile (INH) on mild steel corrosion in 1 M HCl was studied by electrochemical, surface and quantum chemical calculation methods. Results showed that percentage of inhibition efficiency increases on increasing INH concentration. The maximum inhibition efficiency of 96.32% was obtained at 25 mg $L^{-1}$ concentration. Tafel polarization measurements show that the presence of INH in acid solution affects both cathodic and anodic reactions but acts as predominantly cathodic type inhibitor. The Scanning electron microscopy (SEM), energy dispersive X-ray spectroscopy (EDX) and atomic force microscopy (AFM) studies suggest the formation of adherent layer of INH on mild steel surface. The results of theoretical calculations were found to be consistent with the surface and electrochemical results.

## 1. Introduction

Among the several available methods, the use of organic corrosion inhibitors is the most easy and cost effective method to protect metals from corrosion due to their ease and economic synthesis and high inhibition efficiency (Daoud et al., 2015). The organic compounds containing heteroatoms particularly N, O and S either in the ring or in the side chain in addition to multiple bonds (double and triple bonds), all forms of aromatic rings and polar functional groups (such as –OH, –NH$_2$, –CN, –SH, NO$_2$ etc.) act as efficient corrosion inhibitors (Saha et al., 2015). Previous study reveals that organic compounds inhibit metal corrosion by forming a compact and thin film at metal/electrolyte interfaces in which the above polar functional groups act as adsorption centers (Ansari and Quraishi, 2015). The adsorption of these organic corrosion inhibitors on metal surfaces is influenced by a number of factors including nature of metal and testing media, chemical structure of organic inhibitor, nature of substituents present in the inhibitor, presence of additives, solution temperature etc. (Obot et al., 2015). The literature survey revealed that several authors have described the significance of the carbonitriles (compounds containing –CN groups) as corrosion inhibitors for different metals (El Azzouzi et al., 2015; Sudheer and Quraishi, 2015; Verma et al., 2014).

* Corresponding author. Tel.: +91 9307025126; fax: +91 542 2368428.

E-mail addresses: maquraishi.apc@itbhu.ac.in, maquraishi@rediffmail.com (M.A. Quraishi).

The influence of 8,9-bis(4 (dimethylamino)phenyl)benzo[4, 5]imidazo[1,2-a]pyridine-6,7-dicarbonitrile (INH) has been described in the present study using electrochemical impedance spectroscopy (EIS), potentiodynamic polarization, scanning electron microscopy (SEM), energy dispersive X-ray spectroscopy (EDX), atomic force microscopy (AFM) and quantum chemical calculation methods.

## 2. Experimental procedure

### 2.1. Materials and chemicals

All electrochemical and surface studies were performed on mild steel specimens containing 0.076 wt.% C, 0.192 wt.% Mn, 0.012 wt.% P, 0.026 wt.% Si, 0.050 wt.% Cr, 0.023 wt.% Al, and balance with Fe. The specimens and electrolytic solution of 1 M HCl were prepared as described earlier (Verma et al., 2015a).

### 2.2. Synthesis of inhibitor

The investigated INH has been synthesized by a one pot four component reaction as described earlier (Yan et al., 2009) and shown in Fig. 1. Completion of the reaction was checked by disappearance of the starting materials on the TLC plates. The synthesized compounds were characterized by IR (KBr, 1/cm) and $^1$H NMR spectral data. The characterization data of the synthesized compounds are as follows: IR(KBr, 1/cm) 3338, 2960, 2856, 2238, 1663, 1645, 1352, 956, 659, $^1$H NMR (300 MHz, CDCl3, $\delta$, ppm): 2.38, 5.63, 5.85, 7.42–7.68.

### 2.3. Electrochemical experiments

The conventional three electrode glass cell assembly consisting of a pure platinum mesh counter electrode, a saturated calomel reference electrode and mild steel specimen working electrode was used for all electrochemical measurements. Tafel and EIS measurements were carried out using a Gamry Potentiostat/ Galvanostat (Model G-300) with EIS software Gamry Instruments Inc., USA. Echem. Analyst 5.0 software package was applied to fit and analyze all electrochemical data. In polarization measurements, the cathodic and the anodic Tafel slopes were plotted by varying the electrode potential inevitably from $-0.25$ to $+0.25$ V vs. corrosion potential ($E_{corr}$) at a constant sweep rate of 1.0 mV s$^{-1}$. The corrosion current density ($i_{corr}$) was obtained by extrapolating the linear segments of the cathodic and anodic Tafel slopes from which percentage of inhibition efficiency was calculated using the following relation (Verma et al., 2015a,b,2016):
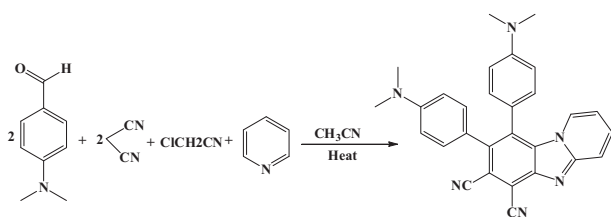
$$\eta\% = \frac{i^0_{corr} - i^i_{corr}}{i^0_{corr}} \times 100 \qquad (1)$$

where, $i^0_{corr}$ and $i^i_{corr}$ are the corrosion current densities in the absence and presence of the INH at different concentrations, respectively.

The electrochemical impedance studies were carried out under potentiodynamic condition in a frequency range of 100 kHz–0.01 Hz. The amplitude of the AC sinusoid wave was 10 mV. All electrochemical studies were performed in naturally aerated solution of 1 M HCl in the absence and presence of different concentrations of INH after a 30 min immersion time. The charge transfer resistances ($R_{ct}$) were calculated from the diameter of the Nyquist plots by which inhibition efficiency at different studied concentrations was calculated using the following relationship (Verma et al., 2016):

$$\eta\% = \frac{R^i_{ct} - R^0_{ct}}{R^i_{ct}} \times 100 \qquad (2)$$

where, $R^0_{ct}$ and $R^i_{ct}$ are the charge transfer resistance in the absence and presence of INH at different concentrations, respectively.

### 2.4. Morphological investigation

For surface study, the mild steel specimens of dimension 1 cm$^2$ were immersed in 1 M HCl for 3 h in the absence and presence of optimum concentrations of INH. After the elapsed time the specimens were taken out washed and cleaned with distilled water, dried and finally analyzed. A SEM model Ziess Evo 50 XVP was employed to carry out SEM analysis. The elements present on the metal surface were studied by energy dispersive X-ray spectroscopy (EDX) coupled with SEM. The atomic force microscopic (AFM) measurements were performed using a NT-MDT multimode AFM, Russia, controlled by Solver scanning probe microscope controller containing NOVA program. The scanning areas were 5 μm × 5 μm during AFM measurements in the absence and presence of the INH.

### 2.5. Quantum chemical calculations

The geometric optimization and theoretical calculations were performed using the density function theory (DFT) method, B3LYP with electron basis set 6–31G* (d, p) for all atoms containing Gaussian 03, E .01 software package (Frisch et al., 2007). In the present study some common quantum chemical parameters namely $E_{HOMO}$, $E_{LUMO}$, $\Delta E$, dipole moment ($\mu$), global hardness ($\rho$) and global softness ($\sigma$) were derived.

## 3. Results and discussion

### 3.1. Electrochemical measurements

#### 3.1.1. Potentiodynamic polarization study

The potentiodynamic polarization nature of mild steel in the absence and presence of the different concentrations of INH is shown in Fig. 2. Several polarization parameters namely corrosion potential ($E_{corr}$), corrosion current density ($i_{corr}$), cathodic ($\beta_c$) and anodic ($\beta_a$) Tafel slopes, surface coverage ($\theta$), and corresponding inhibition efficiency ($\eta\%$) were derived



**Figure 1**  Synthetic scheme for investigated INH.

**Table 1** Tafel polarization parameters for mild steel in 1 M HCl solution in the absence and at different concentrations of INH.

| Inhibitor | Conc (mgL$^{-1}$) | $E_{corr}$ | $i_{corr}$ | $\beta_a$ | $\beta_c$ | $\theta$ | $\eta\%$ |
|---|---|---|---|---|---|---|---|
| Blank | – | −445 | 1150 | 70.5 | 114.6 | – | – |
| INH | 5 | −500 | 293.17 | 74.20 | 191.3 | 0.7450 | 74.52 |
| | 10 | −487 | 186.83 | 60.40 | 159.6 | 0.8375 | 83.75 |
| | 15 | −491 | 118.56 | 78.40 | 186.2 | 0.8969 | 89.69 |
| | 20 | −510 | 72.60 | 86.0 | 127.5 | 0.9369 | 93.68 |
| | 25 | −485 | 42.30 | 63.8 | 125.6 | 0.9632 | 96.32 |

at different INH concentrations and given in Table 1. The results depicted in Table 1 suggest that the values of $i_{corr}$ were significantly decreased in the presence of INH at different concentrations. Results also showed that the decreased in $i_{corr}$ values is more pronounced at high INH concentration. This decrease in $i_{corr}$ values on increasing INH concentration is attributed due to creation of a protective barrier between metal/electrolyte interfaces through adsorption (Feng et al., 2011). From the Tafel plots it is observed that anodic domains did not show any significant change (almost overlapping) over the potential of −350 mV vs SCE. This potential is generally defined as desorption potential. From this it is settled that the corrosion inhibition nature of the INH depends on electrode potential. Generally, it has been reported that the inhibition of the metal corrosion in the presence of inhibitor is associated to the formation of a protective surface film. However, in our present study, the potential higher than −350 mV results in increased rate of metal dissolution due to desorption of INH from the metal surface. Thus it is concluded that over desorption potential the rate of INH desorption increased more than its adsorption. Moreover, from the potentiodynamic results it is observed that cathodic Tafel slopes were comparatively more affected than anodic Tafel slopes. Therefore, finally it is concluded that inhibition of mild steel corrosion in the presence of INH is under cathodic control and it acts as a cathodic inhibitor (Li et al., 2009).

*3.1.2. Electrochemical impedance spectroscopy (EIS) study*

The Nyquist and Bode modulus plots are shown in Fig. 2 (a and b), respectively. From the Nyquist plots it is concluded that diameter of the semicircle increased in the presence of INH. Formation of the semicircle rather than complete circle in the Nyquist plots is attributed due to rough electrode surface resulted from corrosion (Chevalier et al., 2014). Several impedance parameters namely solution resistance ($R_s$), charge transfer resistance ($R_{ct}$), double layer capacitance ($C_{dl}$), phase shift ($n$) and $\eta\%$ were calculated using equivalent circuit shown elsewhere (Verma et al., 2013) and given in Table 2. The double layer capacitance values ($C_{dl}$) were calculated using the following equation (Verma et al., 2015a):

$$C_{dl} = (QR_{ct}^{1-n})^{1/n} \qquad (3)$$

where $Q$ is the constant phase element (CPE) ($\Omega^{-1} Sn$ cm$^{-2}$), and n is the CPE exponent. Generally, the value of $n$ is related to the heterogeneity or roughness of the metal surface. A higher low value of $n$ is generally associated with high surface roughness and heterogeneity. It is observed from the result depicted in Table 2 that the values of $n$ are larger in the presence of INH (0.837–0.869) than in their absence (0.827), suggesting that surface roughness is remarkably improved in the
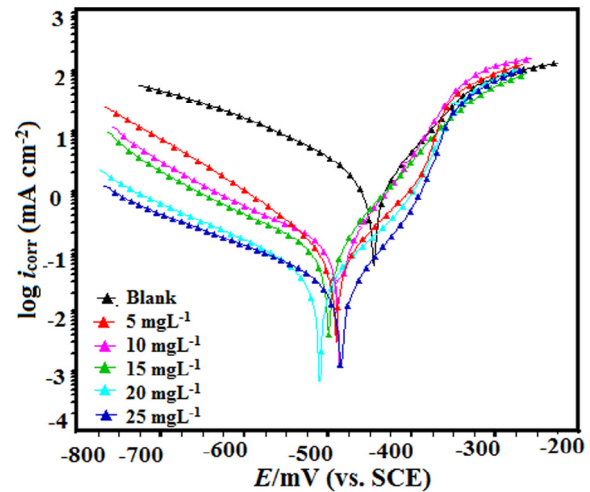


**Figure 2** Potentiodynamic polarization curves for mild in the absence and presence of different concentrations of INH.

**Table 2** EIS parameters obtained for mild steel in 1 M HCl in the absence and presence of different concentrations of INH.

| Inhibitor | Conc (mgL$^{-1}$) | $R_s$ | $R_{ct}$ | $C_{dl}$ | $n$ | $\eta\%$ |
|---|---|---|---|---|---|---|
| Blank | – | 1.12 | 9.58 | 106.21 | 0.827 | – |
| INH | 5 | 0.720 | 38.52 | 89.37 | 0.837 | 75.12 |
| | 10 | 0.737 | 81.85 | 77.56 | 0.844 | 88.32 |
| | 15 | 0.816 | 107.23 | 63.25 | 0.846 | 91.06 |
| | 20 | 0.652 | 196.20 | 59.85 | 0.859 | 95.11 |
| | 25 | 0.760 | 253.83 | 52.51 | 0.869 | 96.11 |

presence of INH owing to the formation of a protective film on mild steel surface by INH (Emran, 2014). Tabulated data suggest that the values of $C_{dl}$ decrease whereas the values of $R_{ct}$ values increase in the presence of INH. The decrease in $C_{dl}$ values is attributed either due to a decrease in local dielectric constant or an increase in the thickness of the electrical double layer or due to a combined effect of both which is resulted due to adsorption of INH at metal/electrolyte interfaces. This decrease in $C_{dl}$ value with an increase in the thickness of the electric double layer can be explained using the Helmholtz model (Verma et al., 2015a):

$$C_{dl} = \frac{\varepsilon\varepsilon_0}{d}S \qquad (4)$$

where $\varepsilon$ is the dielectric constant of the medium, $\varepsilon_0$ is the permittivity of the free space, $S$ is the effective surface area of the working electrode, and $d$ is the thickness of the electric double

layer formed by the adsorbed inhibitor. From the Helmholtz equation it can be concluded that an increase in the thickness of the double layer was responsible for a decrease in $C_{dl}$ values. This finding suggests that INH inhibits mild steel corrosion by adsorbing on its surface (Zhao et al., 2015).

An ideal corroding system is characterized by a constant value of phase angle as $-90°$ having slope value unity. However, a deviation is observed from the ideality in our present study which is due to the rough electrode surface resulted due to accumulation of corrosion products. From the Bode plot (Fig. 3b) it could be observed that values of phase angle have been remarkably improved in the presence of INH as compared to free acid solution. This improvement in the phase angle values suggest that surface smoothness increased in the presence of INH due to the formation of a protective covering on the mild steel surface (Bammou et al., 2014).

## 3.2. Surface investigations

### 3.2.1. SEM measurements

Fig. 4 represents the SEM micrographs of the mild steel surface in the absence and presence of optimum (25 mgL$^{-1}$)

concentration of the INH. The SEM micrograph (Fig. 4a) shows characteristics pits and cracks due to acid corrosion. However, the surface morphology remarkably improved in the presence of INH (Fig. 4b) due to the formation of a protecting surface film.

### 3.2.2. EDX measurements

EDX spectra of mild steel in the absence and presence of optimum concentration of INH ae shown in Fig. 5. The EDX spectrum in the absence of INH shows only two signals corresponding to Fe (iron) and C (carbon). However, in the EDX spectrum of mild steel in the presence of INH (Fig. 5b), an additional signal corresponding to N (nitrogen) was observed which is resulted due to the adsorption of INH on mild steel surface. The percentage of elements present on mild steel surface is represented in Table 3.

### 3.2.3. AFM measurements

Fig. 6 represents the AFM micrographs of mild steel surface in the absence and presence of optimum concentrations of INH
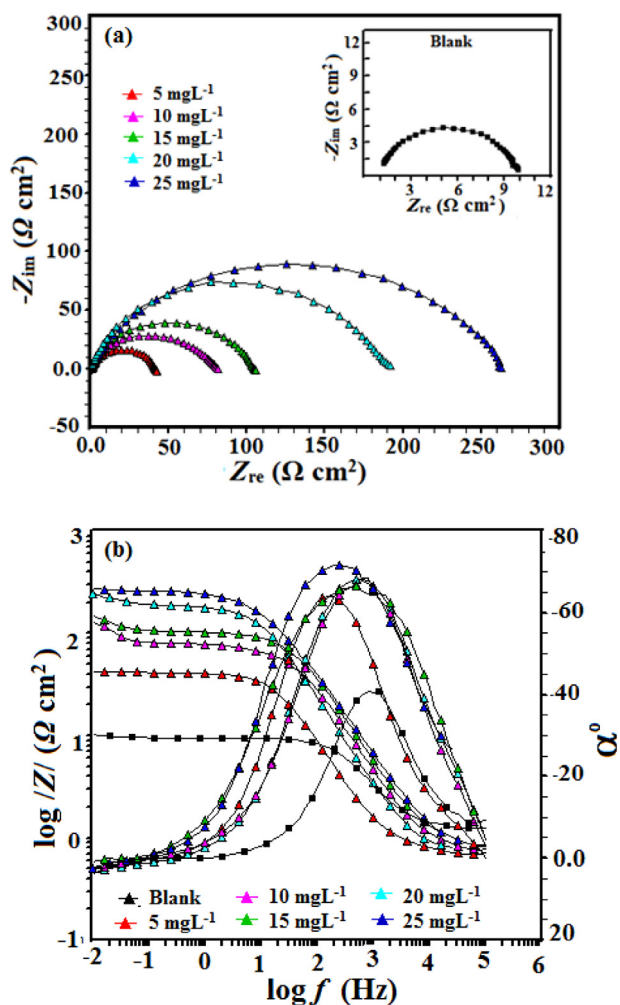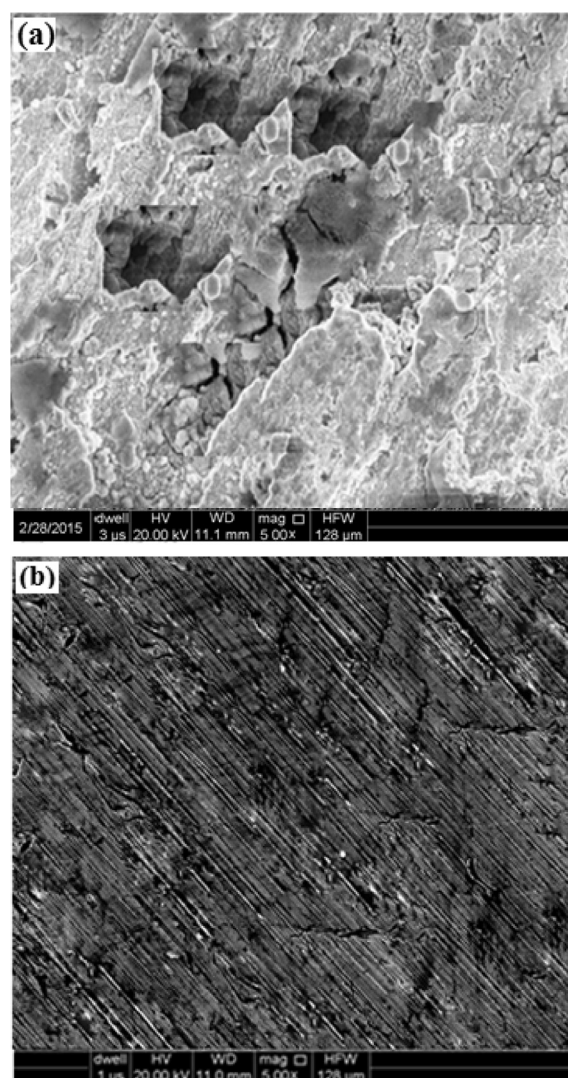


**Figure 3** (a) Nyquist plot for mild steel in 1 M HCl without and with several studied concentrations of INH (b) Bode (log $f$ vs log $|Z|$) and phase angle (log $f$ vs $\alpha^0$) plots for mild steel in 1 M HCl in the absence and presence of different concentrations of INH.



**Figure 4** SEM images of mild steel in 1 M HCl solution after 3 h immersion time: (a) in the absence and in the presence of 25 mgL$^{-1}$ of (b) INH.
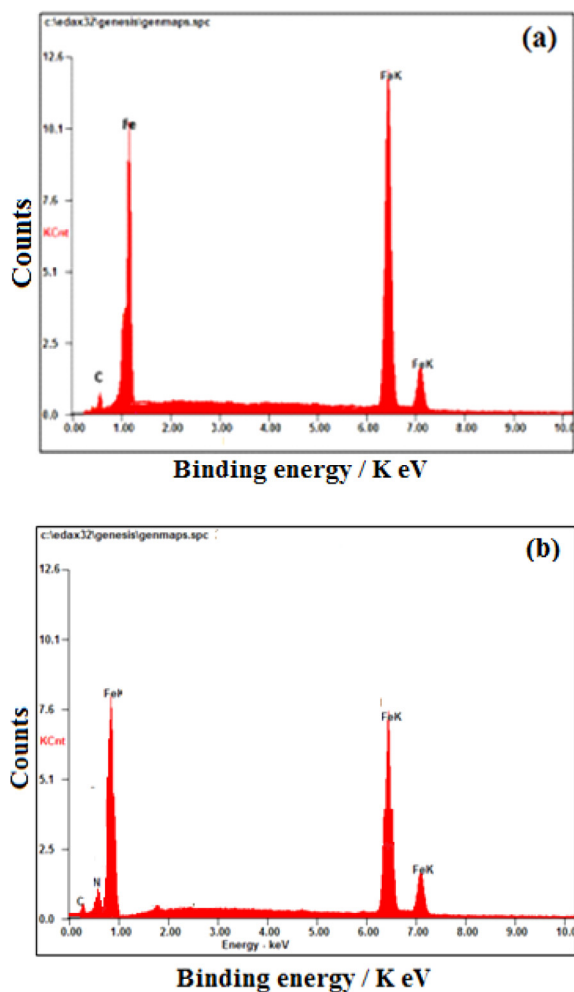
**Figure 5** EDX spectra of mild steel in 1 M HCl solution after 3 h immersion time: (a) in the absence of and in the presence of 25 mgL$^{-1}$ of (b) INH.

**Table 3** Percentage atomic contents of elements obtained from EDX spectra of mild steel with and without INH.

| Inhibitor | Fe | C | N |
|---|---|---|---|
| Blank | 63.09 | 36.10 | – |
| INH | 59.78 | 25.69 | 14.81 |

after 3 h immersion time. The AFM micrograph in the absence of IHN (Fig. 6a) shows a highly rough surface due to acid corrosion. The calculated surface roughness in the absence of INH was 392 nm. However, in the presence of INH at 25 mgL$^{-1}$ concentration (Fig. 6b), the surface roughness is significantly improved due to the formation of a protective film by INH. The calculated surface roughness was 126 nm.

### 3.3. Quantum chemical calculation

Fig. 7(a–c) represents the optimized and frontier molecular pictures of the investigated INH. Several theoretical parameters namely energy of highest occupied molecular orbital ($E_{HOMO}$), energy of lowest unoccupied molecular orbital ($E_{LUMO}$), energy band gap ($\Delta E$), dipole moment ($\mu$), global
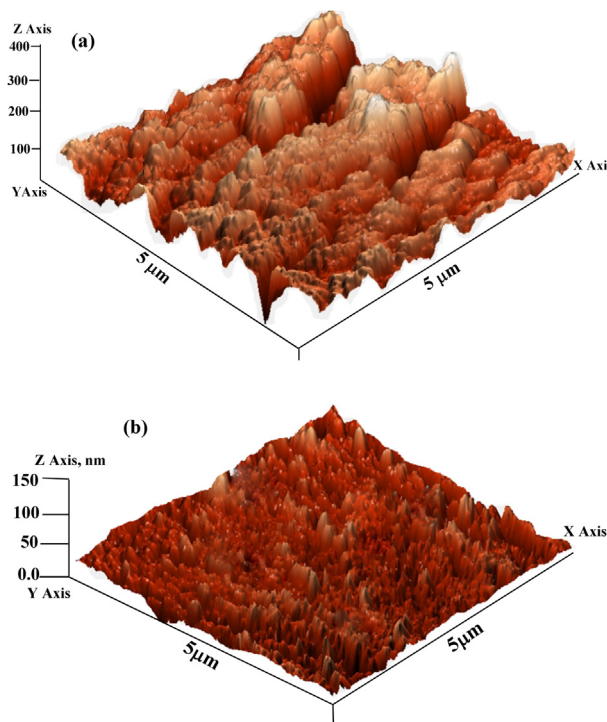




**Figure 6** AFM images of mild steel in 1 M HCl solution after a 3 h immersion time: (a) in the absence of INH and (b) in the presence of 25 mgL$^{-1}$ of INH.

hardness ($\rho$) and global softness ($\sigma$) were calculated and given in Table 4. It is reported that a higher value of $E_{HOMO}$ and a low value of $E_{LUMO}$ are associated with high inhibition efficiency [20]. A very small value of $\Delta E$ (0.09228) in our present case suggests that INH has a strong tendency to adsorb on mild steel (Banerjee et al., 2011). Moreover, the dipole moment of INH is much higher (17.6170 Debye) as compared to the dipole moment of water suggesting that INH has a much stronger tendency to adsorb on the mild steel surface in aqueous acidic solution containing INH (Tang et al., 2009). The global hardness ($\rho$) and softness ($\sigma$) are two other theoretical parameters which can be used to explain the adsorption tendency of the INH. An inhibitor with high value of global hardness and low value of softness is associated with low chemical reactivity and therefore low inhibition efficiency. Generally, the high value of dipole moment and global softness as well as low value of global hardness are associated with high corrosion inhibition efficiency (Ahamad et al., 2010). The compound under taken in the present study has a very small value of hardness and a very high value of softness suggesting that INH is an efficient corrosion inhibitor for mild steel.

### 4. Mechanism of inhibition

The mechanism of mild steel corrosion inhibition in the presence of INH can be explained on the basis of molecular adsorption. The adsorption of an inhibitor at the metal/electrolyte interface takes place by two types of interactions: the physisorption and the chemisorption. Generally, physical adsorption involves electrostatic interactions between charged mild steel surface and charged inhibitor molecule and the chemisorption involves sharing of charges between inhibitor
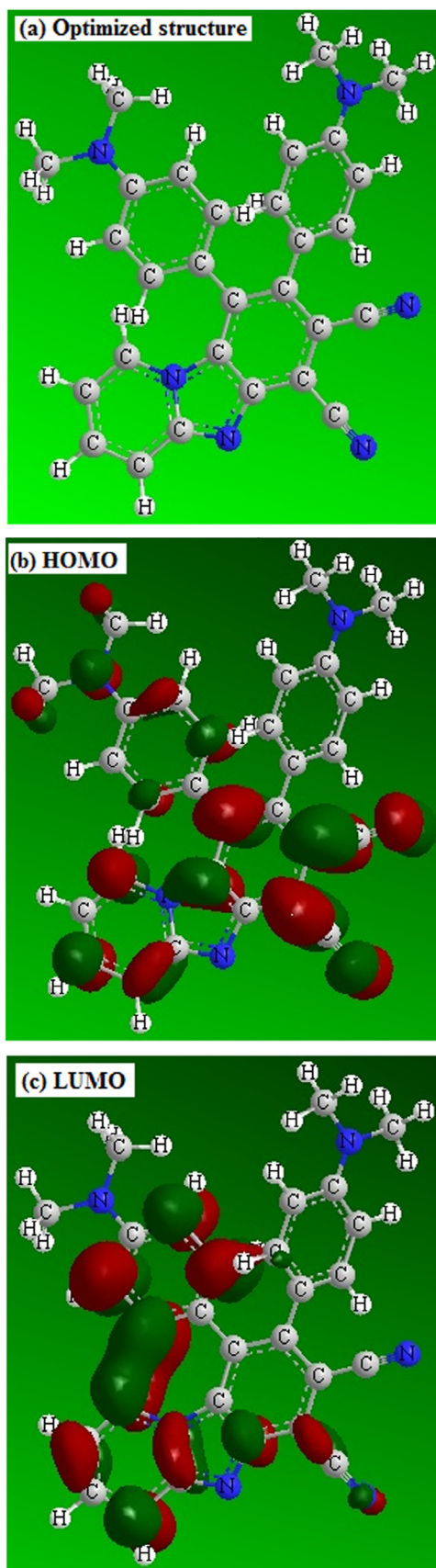
**Figure 7** (a) Optimized molecular structure of INH (b) HOMO frontier molecular orbital density distribution of INH (c) LUMO frontier molecular orbital density distribution of INH.

**Table 4** Quantum chemical parameters for studied INH.

| Compound | $E_{HOMO}$ | $E_{LUMO}$ | $\Delta E$ | $\rho$ | $\sigma$ | $\mu$ |
|---|---|---|---|---|---|---|
| INH | −0.16673 | −0.07445 | 0.09228 | 0.04614 | 21.6731 | 17.6170 |

and metal surface (Verma et al., 2015b). It is reported that the heteroatoms (N, O, S) present in the molecules easily protonate to give a cationic inhibitor. This cationic form of inhibitor electrostatically is attracted by appositively charged mild steel surface. The mild steel surface is negatively charged due to the presence of surface chloride ions (Verma et al., 2015b). Further, initially the cationic form of the inhibitor starts competing with $H^+$ for electrons. However, after release of $H_2$ gas at the cathode, the cationic form of the inhibitor returns in its neutral form. Now, the heteroatoms transfer their electrons in the d-orbital of surface Fe-atoms (donation). However, this type of donation might cause accumulation of extra negative charges on the metal surface. For relief from excessive negative charge, the metal transfers its electrons to the anti-bonding molecular orbital of the INH (Retro-donation). This type of donation and retro-donation strengthen the bonding between metal and inhibitor (Verma et al., 2015b). Moreover, the higher value of dipole moment, low value of global hardness and high value of global softness suggest that the INH has strong tendency to adsorb on mild steel surface in 1 M HCl.

## 5. Conclusion

Present study describes the adsorption behavior of 8,9-bis(4 (dimethyl amino)phenyl)benzo[4,5] imidazo[1,2-a]pyridine-6, 7-dicarbonitrile (INH) on mild steel surface in 1 M HCl using experimental and theoretical techniques. The study suggests that INH is a good corrosion inhibitor for mild steel in 1 M HCl. Results showed that inhibition efficiency increases with increasing concentration of INH. Potentiodynamic polarization study revealed that INH is a mixed type inhibitor. EIS measurements showed that INH inhibits mild steel corrosion by forming a thin surface film between the metal and electrolyte. SEM, EDX and AFM studies conformed the formation of a protective surface barrier. Quantum chemical calculation results were found to be in good support to the experimental results.

### Conflict of interest

The authors have declared no conflict of interest.

### Acknowledgment

### References

Ahamad, I., Prasad, R., Quraishi, M.A., 2010. Adsorption and inhibitive properties of some new Mannich bases of Isatin derivatives on corrosion of mild steel in acidic media. Corros. Sci. 52, 1472–1482.

Ansari, K.R., Quraishi, M.A., 2015. Effect of three component (aniline–formaldehyde and piperazine) polymer on mild steel corrosion in hydrochloric acid medium. J. Assoc. Arab Univ. Basic Appl. Sci. 18, 12–18.

Bammou, L., Belkhaouda, M., Salghi, R., Benali, O., Zarrouk, A., Al-Deyab, S.S., Warad, I., Zarrok, H., Hammouti, B., 2014. Effect of harmal extract on the corrosion of C-steel in hydrochloric solution. Int. J. Electrochem. Sci. 9, 1506–1521.

Banerjee, S., Mishra, A., Singh, M.M., Maiti, B., Ray, B., Maiti, P., Maiti, B., Ray, B., Maiti, P., 2011. Highly efficient polyurethane ionomer corrosion inhibitor: the effect of chain structure. RSC Adv. 1, 199–205.

Chevalier, M., Robert, F., Amusant, N., Traisnel, M., Roos, C., Lebrinia, M., 2014. Enhanced corrosion resistance of mild steel in 1 M hydrochloric acid solution by alkaloids extract from *Aniba rosaeodora* plant: electrochemical, phytochemical and XPS studies. Electrochim. Acta 131, 96–105.

Daoud, D., Douadi, T., Hamani, H., Chafaa, S., Al-Noaimi, M., 2015. Corrosion inhibition of mild steel by two new S-heterocyclic compounds in 1 M HCl: experimental and computational study. Corros. Sci. 94, 21–37.

El Azzouzi, M., Aouniti, A., Herrag, L., Chetouani, A., Elmsellem, H., Hammouti, B., 2015. Investigation of isomers of hydroxyphenylamino propane nitrile as mild steel corrosion inhibitors in 1 M HCl. Der Pharma Chem. 7, 12–24.

Emran, K.M., 2014. Corrosion characterisation and passivation behavior of Fe68.6Ni28.2Mn3.2 alloy in acidic solution. Int. J. Electrochem. Sci. 9, 4217–4229.

Feng, L., Yang, H., Wang, F., 2011. Experimental and theoretical studies for corrosion inhibition of carbon steel by imidazoline derivative in 5% NaCl saturated Ca(OH)$_2$ solution. Electrochim. Acta 58, 427–436.

Frisch, M.J., Trucks, G.W., Schlegel, H.B., Scuseria, G.E., Robb, M.A., Cheeseman Jr., J.R., 2007. Gaussian 03, Revision E.01. Academic Press, Wallingford, CT.

Li, X., Deng, S., Fua, H., Li, T., 2009. Adsorption and inhibition effect of 6-benzylaminopurine on cold rolled steel in 1.0 M HCl. Electrochim. Acta. 54, 4089–4098.

Obot, I.B., Macdonald, D.D., Gasem, Z.M., 2015. Density functional theory (DFT) as a powerful tool for designing new organic corrosion inhibitors. Part 1: an overview. Corros. Sci. 99. http://dx.doi.org/10.1016/j.corsci.2015.01.037.

Saha, S.K., Dutta, A., Ghosh, P., Sukul, D., Banerjee, P., 2015. Adsorption and corrosion inhibition effect of Schiff base molecules on the mild steel surface in M HCl medium: a combined experimental and theoretical approach. Phys. Chem. Chem. Phys. 17, 5679–5690.

Sudheer, Quraishi, M.A., 2015. The corrosion inhibition effect of aryl pyrazolo pyridines on copper in hydrochloric acid system: computational and electrochemical studies. RSC Adv. 5, 41923–41933.

Tang, Y.M., Yang, W.Z., Yin, X.S., Liu, Y., Wan, R., Wang, J.T., 2009. Phenyl-substituted amino thiadiazoles as corrosion inhibitors for copper in 0.5 M H$_2$SO$_4$. Mater. Chem. Phys. 116, 479–483.

Verma, C.B., Quraishi, M.A., Ebenso, E.E., 2013. Electrochemical studies of 2-amino-1, 9-dihydro-9-((2- hydroxyethoxy) methyl)-6H-purin-6-one as Green corrosion inhibitor for mild steel in 1.0 M hydrochloric acid solution. Int. J. Electrochem. Sci. 8, 7401–7413.

Verma, C.B., Quraishi, M.A., Singh, A., 2014. 2-Aminobenzene-1,3-dicarbonitriles as green corrosion inhibitor for mild steel in 1 M HCl: electrochemical, thermodynamic, surface and quantum chemical investigation. J. Taiwan Inst. Chem. Eng. 000, 1–11.

Verma, C.B., Singh, A., Pallikonda, G., Chakravarty, M., Quraishi, M.A., Bahadur, I., Ebenso, E.E., 2015a. Aryl sulfon-amidomethylphosphonates as new class of green corrosion inhibitors for mild steel in 1 M HCl: electrochemical, surface and quantum chemical investigation. J. Mole. Liq. 209, 306–319.

Verma, C.B., Singh, A., Quraishi, M.A., Singh, P., 2015b. A thermodynamical, electrochemical, theoretical and surface investigation of diheteroaryl thioethers as effective corrosion inhibitors for mild steel in 1M HCl. J. Taiwan Inst. Chem. Eng. 58. http://dx.doi.org/10.1016/j.jtice.2015.06.020.

Verma, C.B., Singh, P., Quraishi, M.A., 2016. A thermodynamical, electrochemical and surface investigation of Bis (indolyl) methanes as Green corrosion inhibitors for mild steel in 1 M hydrochloric acid solution. J. Assoc. Arab Univ. Basic Appl. Sci. 21, 24–30.

Yan, C.G., Wang, Q.F., Song, X.K., Sun, J., 2009. One-step synthesis of pyrido[1,2-a]benzimidazole derivatives by a novel multicomponent reaction of chloroacetonitrile, malononitrile, aromatic aldehyde, and pyridine. J. Org. Chem. 74, 710–718.

Zhao, J., Duan, H., Jiang, R., 2015. Synergistic corrosion inhibition effect of quinoline quaternary ammonium salt and Gemini surfactant in H$_2$S and CO$_2$ saturated brine solution. Corros. Sci. 91, 108–119.